Waste and Biomass Valorization (2025) 16:2075–2095
https://doi.org/10.1007/s12649-025-03005-9

ORIGINAL PAPER

Production and Characterization of Densified Briquettes From Nanocomposite Biochar-Cellulose Nanocrystal (Biochar-CNC) Reinforced with Polyvinyl Alcohol (PVA)

Fildah Ayaa[1] · Kabir Oyedotun[2] · Michael Lubwama[1] · Samuel Ayodele Iwarere[2] · Michael Olawale Daramola[2] · John Baptist Kirabira[1]

Received: 16 September 2024 / Accepted: 10 March 2025 / Published online: 22 March 2025

Abstract

Biomass briquettes are still important to communities in developing nations because they are cheap, sustainable, and generated from solid waste that can be utilized to produce energy. However, the low quality of the briquettes when compared to traditional cooking fuels hampers their widespread adoption; yet, there is an opportunity for expanding the briquette market due to the rise in charcoal prices, increasing scarcity of forest resources, and more environmental awareness among consumers. The main objective of this study was to develop a bio-based briquette with improved combustion characteristics through the use of an innovative binder. A novel nanocomposite briquette (biochar/cellulose nanocrystals (CNC)/polyvinyl alcohol (PVA) was produced using the solution casting method, with CNC/PVA nanocomposite as a binder. A total of five (5) nanocomposite briquettes having biochar-to-binder ratios of; 90:10, 80:20, 70:30, 60:40, and 50:50 and designated as *BCP (9/1)*, *BCP (8/2)*, *BCP (7/3)*, *BCP (6/4)* and *BCP (5/5)*, respectively were developed. The nanocomposite briquette samples were characterized for thermal stability, mechanical properties, elemental composition, surface morphology, proximate composition, and combustion characteristics using established methods. The produced briquettes had a very low ash content of less than 2% and a low average moisture content of 8%. The surface morphology of the briquettes revealed a rough and porous structure that can enhance combustion. The *BCP (9/1)* briquette had the highest calorific value of 27 MJ/kg, followed by *BCP (8/2)* and *BCP (7/3)* which had a calorific value of 26 MJ/kg. The *BCP (7/3)* nanocomposite briquette was the most thermally stable, with the lowest onset degradation temperature (220 °C), highest peak temperature (514 °C), least char residue, and the most compressive strength of 11 MPa. The *BCP (9/1)*, *BCP (8/2)*, *and BCP (7/3)* nanocomposite briquettes also satisfied the combustion indices criteria, demonstrating their potential to replace coal in industrial applications. The thermal degradation and kinetics of the nanocomposites were studied using TGA-DTG techniques at three different heating rates; 5 °C/min, 10 °C/min, 20 °C/min in an oxygen environment. The kinetic parameters, that is, the activation energy and pre-exponential factor were calculated using the Coats-Redfern method. The combustion of the briquettes happened in three distinct phases with a higher activation energy required at higher heating rates to initiate the first stage of combustion. Also, up to 40% of the binder can be added without affecting the ignition, combustion, and burn-out properties of the briquette. This study, therefore, demonstrates that Biochar-PVA-CNC nanocomposite briquettes are a potential biofuel for industrial and household applications.

Keywords Biomass waste · Briquettes · Cellulose nanocrystals · Biochar · Nanocomposites · Binder · SDG 7

✉ Michael Olawale Daramola
Michael.Daramola@up.ac.za

[1] Department of Mechanical Engineering, School of Engineering, Makerere University, P.O. Box 7062, Kampala, Uganda

[2] Sustainable Energy and Environment Research Group (SEERG), Department of Chemical Engineering, Faculty of Engineering, Built Environment and Information Technology, University of Pretoria, Hatfield, Pretoria 0028, South Africa

Abbreviations

AENOR	Asociacion Espanola de Normalizacion y Certificacion
CNC	Cellulose nanocrystals
IEA	International Energy Agency
IRENA	International Renewable Energy Agency
KEBS	Kenya Bureau of Standards

PVA	Polyvinyl alcohol
TBS	Tanzania Bureau of Standards
UNBS	Uganda National Bureau of Standards
UNSD	United Nations Statistics Division
WB	World Bank Group
WHO	World Health Organization
N_2	Nitrogen

Introduction

One-third of the world's population, or nearly 3 billion people, still lack access to clean cooking solutions such as electricity, liquified petroleum gas (LPG), and biomass pellets among others [1]. The use of inefficient, polluting fuels and technologies is a health risk and a major contributor to diseases and deaths, particularly for women and children in low- and middle-income countries [1, 2]. The inefficient combustion of solid fuels (wood, coal, charcoal, dung, and crop waste) and kerosene in simple stoves and devices produces high levels of household air pollution (HAP) [1, 3]. Household air pollution was responsible for an estimated 3.2 million deaths per year in 2020, including over 237,000 deaths of children under the age of five [4]. Households relying on polluting energy systems face burdens like time-consuming fuel collection trips, which pose health risks and perpetuate gender and socioeconomic inequities, particularly for women and children [1]. Furthermore, polluting cooking practices are an important cause of environmental degradation and climate change: the black carbon from cooking, heating, and lighting is responsible for 25% of anthropogenic global black carbon emissions, and around 30% of wood fuels harvested globally are unsustainable [1, 5, 6].

The transition to clean cooking fuels in middle- and low-income countries requires intermediate solutions that are sustainable, affordable, and meet the sociocultural cooking needs of people. In the medium term, sustainable cooking solutions compatible with these communities' cooking practices must be developed. Briquettes from carbonized or densified biomass are promoted widely in low-income countries as an alternative to fuel wood and charcoal for cooking fuels [7]. Utilization of agricultural residues as a primary source of raw material in the development of briquettes as alternative cooking fuels presents a significant opportunity to develop sustainable cooking fuels, while at the same time handling the waste management and environmental challenges that arise when these agricultural residues are left to rot or burned in open fields [7, 8].

Briquettes from different agricultural residues have been widely researched and developed [7–20]. In this study, waste branches from *Senna spectabilis* (commonly known as cassia) and *Hyparrhenia filipendula* (commonly known as yellow thatching grass) were used. Cassia is widely cultivated as a boundary marker and has also colonized natural forests and forest reserves in Uganda [21]. The timber from cassia is not valuable but it has potential to produce good quality charcoal [22]. Additionally, *Hyparrhenia filipendula* is a grass that is commonly found in the cattle corridor of Uganda. The grass is mainly used for roofing houses, and grazing cattle in its early stages of growth [23]. It is common practice to burn mature plants, posing fire and health- related hazards. This study therefore investigated the potential of utilizing these two biomass sources for production of a biomass-based briquette.

Carbonized briquettes, primarily composed of biochar, are reported to have a higher calorific value than uncarbonized briquettes [15]. However, biochar requires a binder, especially when compacted at low pressure, or manually, to improve the mechanical and thermal properties of the briquettes. Briquette binders are generally classified into inorganic, organic, and composite binders [24]. The poor thermal stability of organic binders (such as biomass, tar pitch, petroleum bitumen, lignosulphonate, and polymers) limits their commercial application in biomass briquetting [24]. Inorganic binders (such as clay, bentonite, ammonium nitrate, etc.) have lower combustion efficiency and high ash content [24]. Composite binders often yield briquettes with high mechanical strength and thermal stability [9, 24–27]. However, the composite binders are still characterized by high ash content, low thermal stability, and high cost [9].

Nanocomposites present a promising avenue for the development of innovative and sustainable binder materials for biomass briquettes. Specifically, polymer nanocomposites incorporating renewable fillers like nanocellulose offer the potential to create cost-effective and environmentally-friendly binder solutions. Polyvinyl alcohol (PVA), a long-chain structural polymer, has been previously utilized both as a binder and in composite binders due to its good viscosity, compatibility, and biodegradability [28–33]. Nanocellulose, derived from biomass and biomass waste, is equally attractive due to its abundance, renewability, and biodegradability, making it a valuable component in the development of sustainable composite binders. However, the development of PVA/Cellulose nanocrystal (CNC) nanocomposite binders for briquetting has been lightly explored in literature. Therefore, the objective of this study was to investigate the properties of briquettes produced with a PVA/CNC binder.

As far as could be ascertained, the preparation of nanocomposite biochar-PVA-CNC materials for briquettes has not been addressed in literature until now. In this study, we investigate the use of a PVA/cellulose nanocrystal (CNC) nanocomposite as a binder for biochar briquettes

and evaluate the properties of the resulting briquettes. This approach not only aims to produce high-quality biomass fuel but also has the potential to stimulate the growth of intermediate industries focused on producing high-value products like nanocellulose from inexpensive and readily available biomass and biomass waste. Furthermore, by leveraging established formulations and materials, the production of biomass briquettes can be upscaled, contributing to the broader adoption of sustainably harvested renewable energy sources for cooking.

Materials and Methods

Materials

Two types of biomass were used in this study: *Senna spectabilis* (commonly known as cassia) for the biochar and *Hyparrhenia filipendula* (commonly known as yellow thatching grass) for the CNC. The branches of *Senna spectabilis* were collected from Mabira Forest in Buikwe District, Uganda, in January 2021. The *Hyparrhenia filipendula* grass was harvested in the wild from Palabek Kal in Lamwo District, Uganda, in July 2022. The following reagents were used without further purification; Polyvinyl alcohol (MW 89,000–98,000, 99% hydrolyzed), sodium hydroxide (98%, AR), toluene (90%, AR), glacial acetic acid (99%, AR), Sodium chlorite (80%, AR), Hydrochloric acid (37%, AR) purchased from Sigma-Aldrich, South Africa; and citric acid monohydrate (99.8%) from Glassworld, & Chemical Suppliers CC, Maraisburg, South Africa.

Synthesis of CNCs from *Hyparrhenia filipendula*

The *Hyparrhenia filipendula* grass was dried in the oven at 100 °C for 2 h. The dried blades and sheaths were removed to expose the culm that was used in subsequent processes. The culm was cut into small pieces of lengths of about 1–2 cm, shredded in a blender, and milled using a PM 100 ball mill (Retsch, Germany) for 3 h, with 10 mm diameter stainless steel grinding balls at 300 rpm. The fibers were then passed through a 38 µm sieve and stored in an air-tight container to prevent degradation of the sample. The extractives were removed using a Soxhlet extractor at 110 °C for 4 h with toluene/ethanol (2:1 v/v). The extractive-free straws were then washed with de-ionized water and ethanol, and dried at 45 °C for 2 h.

The pulping of the extractive-free stems was carried out at 100 °C for 4 h in a Parr reactor using 10 wt % NaOH and liquor to solid ratio of 15:1 (v/w). The pulp was extracted after the cooking time via vacuum filtration and washed several times with deionized water until a neutral pH was obtained. The pulp was then dried in the oven at 45 °C for 2 h and stored for further analysis. 2 g of the pulp was then bleached using acidified sodium chlorite (1.2 g Sodium chlorite, 0.3 mL acetic acid, and 100 mL deionized water) at 95 °C for 4 h in a Parr reactor. The bleached pulp was washed with deionized water until a neutral pH was obtained. The filtrate was dried at 45 °C for 1 h. These pre-treatment conditions, previously reported in our work, have been identified as the most effective [23]. The cellulose fibers were then hydrolyzed using 80 wt % citric acid, with an acid-fiber ratio of 2:1 for 4 h in a Parr reactor at 120 °C. The acid hydrolysis conditions were adjusted based on previous studies and preliminary investigations [34, 35]. The precipitate was dialyzed in de-ionized water for 3 days with up to four water changes per day until a neutral pH was obtained. The sample was then sonicated in an ice bath for 2 h in a 480 W PS-80 Ultrasonic cleaner and homogenized using an HG-15D homogenizer at 10,000 rpm for 5 min. The sample was then frozen at −40 °C for 12 h and freeze-dried for 72 h. The lyophilized CNCs were stored in an air-tight container for further analysis.

Preparation of Biochar

The branches of *Senna Spectabilis* were sun-dried for two weeks. The branches were then cut into small pieces with lengths of about 3–4 cm, washed with ethanol, and dried. The samples were then pyrolyzed at 350 °C for 1 h in a horizontal tube furnace (BR-12NT Vacutec Brothers) under the flow of nitrogen gas at a flow rate of 200 mL/min. This pyrolysis condition was selected based on findings from our previous study [22]. The biochar obtained was milled using a Retsch PM 100 ball mill for 3 h at 300 rpm and passed through a 38 µm sieve. The biochar was then leached in a solution of acetic acid and hydrochloric acid (3:1 v/v) at 80 °C for 24 h with constant stirring at 400 rpm. The sample was then washed with 1 M hydrochloric acid and deionized water until a neutral pH was reached and air-dried for 12 h.

Preparation of CNC-PVA-Biochar Composite

A 10 wt % PVA solution was prepared by constantly stirring at 300 rpm for 2 h at 100 °C until the PVA was completely dissolved. The solution was cooled and stored in an airtight container. The PVA solution was mixed with a 10 wt % CNC suspension and agitated for 1 h in an oil bath inside a Teflon cup at 100 °C. The mixture was stirred for an additional hour while a measured amount of biochar was gradually added. The resulting slurry was left to air-dry for 12 h before being compacted at room temperature using a manual Servex hydraulic press (HP 15) with a capacity of 150 kN in a custom-made cylindrical steel mold with an internal

Table 1 Ratios used for nanocomposite sample Preparation

Sample designation	Bio-char, g	CNC, g	De-ionized water, mL	10 wt % PVA, mL	Bio-char: CNC ratio
BCP (9/1)	9	1	10	10	90:10
BCP (8/2)	8	2	20	20	80:20
BCP (7/3)	7	3	30	30	70:30
BCP (6/4)	6	4	40	40	60:40
BCP (5/5)	5	5	50	50	50:50

diameter of 15 mm and height of 50 mm. A compressive pressure of 40 MPa was used. The densified product was dried at 100 °C for 2 h and stored in an airtight container for further use. The mixing ratios for the materials used and sample designation are shown in Table 1. A summary of the experimental procedure is shown in Fig. 1.

Physicochemical Measurements

The moisture, ash, and volatile content of the samples were determined by using a Thermo-gravimetric analyzer (Eltra Thermostep), following the ASTM E1131-20 standard procedure. The fixed carbon content is calculated according to Eq. 1.

$$FC\,(\%) = 100 - (\%Ash\ +\ \%VM) \tag{1}$$

Where % FC, %Ash, and %VM, are the mass percentages of fixed carbon, ash, and volatile matter of the samples respectively.

The ultimate analysis was determined using an Elementar UNICUBE. The Oxygen content was determined using Eq. 2

$$O\,(wt\%) = 100\,(wt\%) - C\,(wt\%) - H\,(wt\%) - N\,(wt\%) - S\,(wt\%) \tag{2}$$

The morphology and elemental composition of the samples were examined using a Zeiss Ultra Plus FEG Scanning electron microscope equipped with an energy-dispersive X-ray spectroscope (EDS). The samples were coated with carbon using a Quorum Q150T ES sputter coater to enhance image resolution. The samples were also placed on a silver tape and coated with gold at 25 mA for 2 min for EDS analysis. Functional groups in the samples were determined by Fourier transform infrared spectroscopy (FT-IR) in the medium infrared region of 4000–400 cm^{-1} with a Bruker Alpha FTIR spectroscope. The thermal stability of the samples was determined using a Thermogravimetric analyzer (Eltra Thermostep). The thermogravimetry (TG) and derivative thermogravimetry (DTG) curves were recorded from the ambient temperature to 1000 °C at a constant heating rate of 10 °C/min under a nitrogen atmosphere. The heating value of the biomass was determined using an adiabatic oxygen bomb calorimeter (IKA C2000 automated digital calorimeter) according to the ASTM D5865-13 standard test method. The mechanical properties of the nanocomposite fuels were evaluated using a Testometric FS300CT Universal testing machine. A micrometer gauge was used to measure the dimensions of each sample before testing. The measurements were also performed at a strain rate of 6 mm/min. The combustion experiments were carried out using an Eltra Thermostep thermal gravimetric analyzer in an Oxygen environment at three different heating rates of 20 °C/min, 10 °C/min, and 5 °C/min.

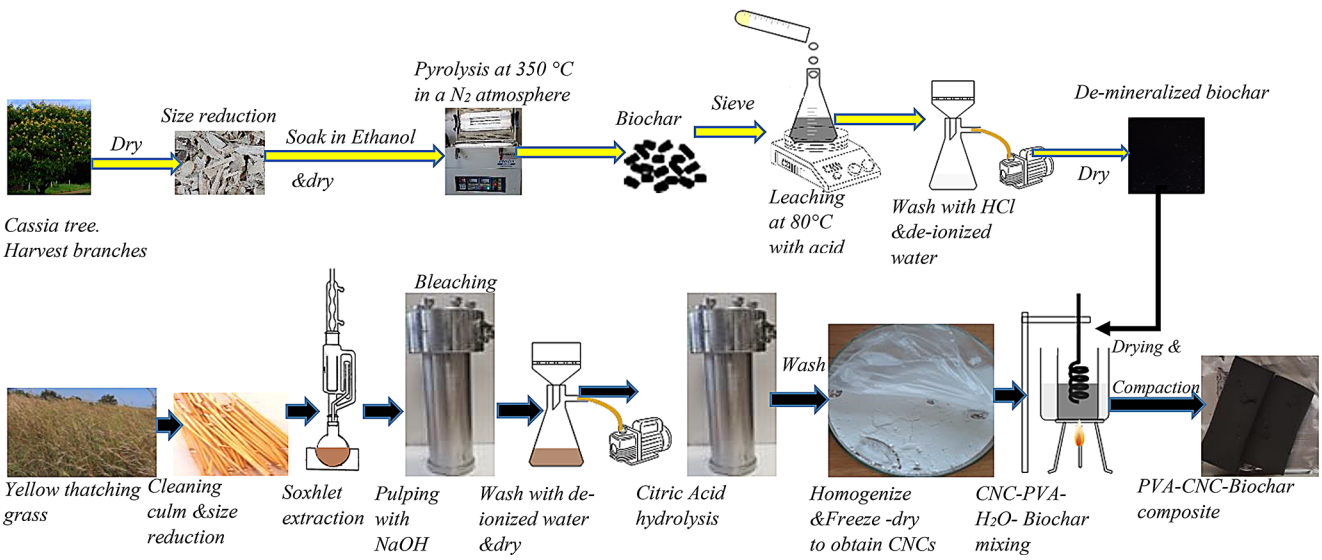

Fig. 1 Summary of experimental procedure

Combustion Indices

To assess the utility of the nanocomposite fuel, the fuel ratio (FR), combustibility index (CI), and volatile flammability (VI) were calculated according to Conag et al. using the following Eqs. [36, 37].

$$Fuel\ ratio, FR = \frac{FC_{db}}{VM_{db}} \tag{3}$$

$$\text{Combustibility index}, CI = \frac{HHV_{db}}{FR} \times (115 - Ash_{db}) \times \frac{1}{105} \tag{4}$$

$$Volatile\ ignitability, VI = \left(\frac{HHV_{db} - 0.338FC_{db}}{VM_{db} + M_c}\right) \times 100 \tag{5}$$

$$HHV_{db} = \left(\frac{HHV}{100 - M_c}\right) \times 100 \tag{6}$$

Where FC is fixed carbon content, VM is volatile matter content, HHV is higher heating value, M_C is the moisture content and db is dry basis.

The ignitability index (I_I) is calculated from Eq. 7 [38].

$$I_I = \frac{HHV - 81FC_{db}}{VM_{db} + MC} \tag{7}$$

Where HHV is the calorific value of the fuel (kJ/kg), FC is the fixed carbon (%), VM is the volatile matter (%) and MC is the moisture content.

The data points of the TG-DTG profiles were also used to determine the ignition index (D_i), burnout index (D_f), combustion performance index (S), index of intensity (H_f), and flammability index (C), during combustion using the following equations [39].

$$D_i = \frac{DTG_{max}}{t_i t_p} \tag{8}$$

$$D_f = \frac{DTG_{max}}{t_p t_f \Delta t_{\frac{1}{2}}} \tag{9}$$

$$S = \frac{DTGmean \times DTGmax}{{T_i}^2 T_f} \tag{10}$$

$$H_f = T_P In \left(\frac{\Delta t_{\frac{1}{2}}}{DTG_{max}}\right) (10)^{-3} \tag{11}$$

$$C = \frac{DTG_{max}}{T_i^2} \tag{12}$$

Where DTG_{max} is the maximum combustion rate (mg min^{-1}), t_i is the ignition time (min), tp is the corresponding time of DTG_{max} (min), t_f is the burnout time (min), $\Delta t_{1/2}$ is the time range of $DTG/DTG_{max} = 0.5$ (min), DTG_{mean} is the mean combustion rate (mg min^{-1}); $\Delta T_{1/2}$ is the temperature range of $DTG/DTG_{max} = 0.5$ (K), Tp is the peak temperature (K), ignition temperature T_i(K), and burnout temperature T_f (K).

The average burning rate can also be calculated from Eq. 13 [40, 41];

$$DTG_{mean} = \left(\frac{\alpha_i - \alpha_f}{T_f - T_i}\right) \times \beta \tag{13}$$

Where β is the heating rate, α_i is the remaining sample percentage corresponding to the ignition temperature point, α_f is the remaining sample percentage corresponding to the burnout temperature point (%).

The ignition index and combustion index can then be calculated from Eqs. 14 and 15 respectively.

$$D_i = \frac{DTG_{max}}{T_f T_i} \tag{14}$$

Where DTG_{max} is the maximum combustion rate (% min^{-1}), T_i is the ignition temperature (K), and T_f is burnout temperature (K).

$$S = \frac{DTGmean \times DTGmax}{{T_i}^2 T_f} \tag{15}$$

Where S is the index of comprehensive combustion characteristic ($min^{-2} \cdot K^{-3}$). Equations 13,14 and 15 are more convenient to use to determine the comprehensive combustion characteristic and ignition index, as the values can be directly obtained from the TG and DTG curves using the tangent method.

Combustion Kinetics

The combustion kinetics of the nanocomposite briquettes was analyzed using the First order Arrhenius law, which governs biomass combustion kinetics, as stated in Eq. 16 [42];

$$\frac{d\alpha}{dt} = K(T) f(\alpha) = Aexp\left(\frac{-E}{RT}\right) f(\alpha) \tag{16}$$

Where T is the absolute temperature (K), R is the universal gas constant (8.314 J K^{-1} mol^{-1}), E is the

activation energy (kJmol^{-1}), A is the preexponential factor (min^{-1}) of the reaction; *f(α)* is the conversion function, α is the conversion rate, which represents the relationship between the initial mass m_o, final mass m_∞ and the mass of the sample at any time t during the experimental run, m_t of the system as given Eq. 17.

$$\alpha = \frac{m_o - m_t}{m_o - m_\alpha} \tag{17}$$

When the heating rate $\beta = \frac{dT}{dt}$ is constant, Eq. 16 can be integrated as follows:

$$g(\alpha) = \int_0^\alpha \frac{d\alpha}{f(\alpha)} = \frac{A}{\beta}\int_0^T dT exp\left(\frac{-E}{RT}\right) \tag{18}$$

Where *g(α)* is an integration function and the integral can be approximated to Eq. 19.

$$In\left[\frac{g(\alpha)}{T^2}\right] = In\left[\frac{AR}{\beta E}\left(1 - \frac{2RT}{E}\right)\right] - \frac{E}{RT} \tag{19}$$

The Coats–Redfern method was used to determine the Arrhenius parameters, in which case.

$f(\alpha) = (1-\alpha)$ and $g(\alpha) = -In(1-\alpha)$, and RT/E $\ll$ 1, thus 1 − RT/E ≈ 1 thus the kinetic mechanism equation for the combustion process can be described by Eq. 20.

$$In\left[\frac{-In(1-\alpha)}{T^2}\right] \approx In\frac{AR}{\beta E} - \frac{E}{RT} \tag{20}$$

The left-hand side of the equation is plotted against 1/T, and the resulting linear relationship enables the determination of the activation energy (E) from the slope of the line, while the pre-exponential factor (A) can be obtained from the intercept. The slope of the line is equal to - $\frac{E}{RT}$ and the intercept of the straight line is equal to $In\left[\frac{AR}{\beta E}\right]$.

Results and Discussion

Proximate Analysis

The proximate analysis of the nanocomposite fuels and starting materials is shown in Table 2. The moisture content was 8% for briquettes, 4% for biochar, and 10% for CNC. According to the South African Bureau of Standards (2000), the Kenya Bureau of Standards (2020), and the Tanzania Bureau of Standards (2022), the recommended moisture content of carbonized briquettes should not exceed 10% [43–45]. Therefore, all of the briquettes meet these criteria. A low moisture content in the briquettes enhances their suitability as a fuel, as it reduces the energy required for the evaporation phase and minimizes smoke production during combustion [7]. Furthermore, the moisture content of all samples is less than 18%, indicating all the samples contained chemically bound water in their structure [43].

According to the Kenya Bureau of Standards (2020), and the Tanzania Bureau of Standards (2022), the ash content of carbonized briquettes should not exceed 27%. The ash content of all the briquettes prepared in this study is less than 2%, with *BCP (7/3)* having the lowest ash content of 0.87%,

Table 2 Proximate analysis of selected samples

Sample	As-received basis, %				Dry basis, %			Reference
	Moisture	Fixed carbon	Volatile matter	Ash	Fixed carbon	Volatile matter	Ash	
BCP (9/1)	6.91±0.39	29.86±6.70	61.82±6.54	1.41±0.23	36.66±0.00	61.84±7.24	1.50±0.25	This study
BCP (8/2)	7.55±0.04	32.63±2.84	58.44±2.81	1.38±0.00	35.66±0.00	62.85±3.04	1.49±0.00	
BCP (7/3)	7.84±0.12	26.32±0.93	64.96±0.96	0.87±0.1	29.00±0.00	70.06±0.96	0.94±0.11	
BCP (6/4)	7.90±0.11	19.67±2.14	71.4±2.31	1.02±0.05	21.85±0.00	77.04±2.41	1.11±0.06	
BCP (5/5)	7.84±0.19	15.79±3.55	74.92±3.12	1.45±0.62	17.65±0.00	80.79±3.23	1.56±0.66	
Biochar	6.75±0.00	16.65±0.00	74.25±0.00	2.35±0.00	18.22±0.00	79.27±0.00	2.51±0.00	
De-mineralized biochar	4.81±0.47	41.61±4.87	53.27±5.09	0.36±0.21	56.63±6.21	42.83±4.87	0.54±0.29	
CNC	10.40±0.62	0.26±0.09	89.09±0.81	0.24±0.11	3.23±0.09	95.32±1.56	1.45±0.20	
Briquettes from wheat straw waste	-	-	-	-	22.45±2.11	68.44±5.47	9.11	[70]
Wood charcoal	5.39	73.3	24.8	1.85	-	-	-	[43]
Charcoal briquettes from molasses, clay, and bagasse mixed in a ratio of 1:1:40 respectively	4.10	36.40	27.20	36.40	-	-	-	[43]
Briquettes from carbonized groundnut shells and cassava starch binder	7.5	53.6	28.4	10.5	-	-	-	[7]
Briquettes from carbonized bagasse and cassava starch binder	6.6	49.8	33.4	10.2	-	-	-	[7]

thereby meeting the required criteria for charcoal briquettes. The briquettes also meet the more stringent European EN 1860-2 and German DIN 51,749 standards, which require an ash level of no more than 8% on a dry basis for charcoal briquettes [46]. Moreover, the low ash content of the briquettes is desirable, as it minimizes dust emissions that contribute to air pollution during combustion. High ash content in solid fuels can lead to increased particulate matter emissions, reduced combustion efficiency, and frequent maintenance issues due to ash buildup in combustion systems. Additionally, lower ash content improves fuel quality by enhancing calorific value and reducing the amount of residual waste after burning, making the briquettes more environmentally-friendly and suitable for clean energy applications [47–49].

The lowest volatile matter obtained in this study was 62% for *BCP (9/1)* while the highest volatile matter was 81% for *BCP (5/5)*. The volatile matter in the briquettes increased as the CNC content increased. This is the expected result because of the substitution of carbonized agricultural residues with the PVA/CNC binder [7]. Furthermore, the recommended volatile matter content for carbonized briquettes is 25 −27%, hence all the briquettes would not meet this criterion [44, 45, 50]. However, European standards for charcoal briquettes do not specify a minimum or maximum value for volatile matter [46]. Solid fuels with a low volatile matter are easier to ignite, burn smoothly and have a longer combustion duration. This is because low volatile matter fuels undergo slower thermal decomposition, leading to a more controlled release of gases and a steadier flame. Additionally, they produce less smoke and fewer emissions compared to high volatile matter fuels, which release a large amount of gaseous compounds rapidly upon heating. A lower volatile matter content also enhances the fuel's thermal efficiency and stability, making it more suitable for applications requiring sustained heat output, such as industrial furnaces and residential heating systems [51–54]. The briquette formulations should be optimized to achieve a lower volatile matter content to comply with the East African regional standards for carbonized briquettes.

The highest fixed carbon content obtained in this study was 37% for *BCP (9/1)* while the lowest fixed carbon content was 18% for *BCP (8/2)*. The fixed carbon content also decreased with an increase in the amount of the binder in the briquettes, thereby showing an agreement with literature [55, 56]. The European EN 1860-2 European standard requires a minimum fixed carbon content of 75%, the Tanzanian MEDC 12 (1323) DTZS and Kenyan DKS2912: 2020 norms require a minimum of 44%, and US 765: 2007 Ugandan Standard mandates a minimum 60% fixed carbon content for carbonized briquettes [44, 45, 50, 57]. The briquettes do not meet any of the standards based on this criterion. If greater commercial value is to be obtained from the nanocomposite briquettes, the formulations should be adjusted with materials with higher fixed carbon content like coke or petroleum coke. With Uganda's upcoming petroleum refining operations, petroleum coke presents a potential feedstock for solid fuel production [58].

As demonstrated in Table 2, the briquettes produced during this study generate a lower amount of ash compared to agricultural residues mentioned in previous studies. The moisture and ash content are within acceptable limits, indicating that the generated briquettes are suitable for cooking applications. However, further optimization of volatile matter and fixed carbon content is necessary for improved commercial and ecological viability of the briquettes. Incorporating materials with a high fixed carbon content into the briquette formulation can enhance its fixed carbon content while reducing volatile matter. However, this modification may lead to increased production costs of the briquettes.

Ultimate Analysis

The ultimate analysis is shown in Table 3. The *BCP (9/1)* nanocomposite fuel sample has the highest carbon content, and least oxygen content, indicating a high energy density of the briquette. Also, the carbon content decreased with an increase in the binder, while the oxygen content increased, in line with published literature [59]. The nanocomposite briquettes exhibit a higher carbon content compared to other reported briquettes with organic binders, resulting in higher combustion quality [60]. The results in Table 3 and findings from other authors consistently demonstrate that higher oxygen content in briquettes tends to decrease their higher heating value (HHV) [61, 62]. Minimal Sulphur and Nitrogen contents indicate that the thermal conversion of the fuel results in low concentrations of nitrogen oxides (NO_X) and Sulphur oxides (SO_X) [62].

The H/C and O/C ratios play a significant role in determining the fuel properties and combustion behavior of biomass fuel samples. The nanocomposite fuels had comparable ranges for the H/C and O/C ratios, with H/C ratios ranging from 1.23 to 0.8 and O/C ratios ranging from 0.27 to 0.42. A fuel with low atomic ratios of O/C and H/C is highly preferred because it produces less smoke, water vapour, and energy loss during combustion [63, 64]. Briquettes with a H/C ratio less than 1.5 and an O/C ratio below 0.8 are considered highly flammable [65]. Given that all the nanocomposite briquettes in this study meet these criteria, they demonstrate high flammability, making them suitable for efficient energy generation with improved combustion performance. Furthermore, it can be observed from Table 3, as well as corroborated by the findings of other researchers, that fuels characterized by low atomic O/C and H/C ratios exhibit higher HHV [66–68].

Table 3 Ultimate analysis of selected samples

Sample	Mass composition: dry-ash-free (daf) basis					H/C	O/C	O_2 consumption	Air required for combustion	HHV	LHV	Reference
	C [%]	H [%]	O [%]	*N* [%]	S [%]	(mol_H mol_C^{-1})	(mol_O mol_C^{-1})	(kg/kg_{fuel})	(kg/kg_{fuel})	MJ kg^{-1}	MJ kg^{-1}	
BCP (9/1)	68.99	4.62	24.73	1.66	0.00	0.80	0.27	1.85	7.98	27.6	26.6	This study
BCP (8/2)	66.81	4.94	26.64	1.38	0.23	0.88	0.30	1.81	7.79	26.9	25.8	
BCP (7/3)	64.14	5.06	29.24	1.26	0.30	0.94	0.34	1.73	7.46	25.6	24.5	
BCP (6/4)	60.65	5.30	32.65	1.41	0.00	1.04	0.40	1.63	7.01	24.1	22.9	
BCP (5/5)	59.77	6.16	33.20	0.87	0.00	1.23	0.42	1.67	7.18	24.5	23.1	
Biochar	76.73	4.62	16.85	1.80	0.00	0.72	0.16	2.11	9.09	31.7	30.7	
CNC	43.86	5.32	49.20	1.28	0.34	1.44	0.84	1.06	4.58	15.5	14.3	
Briquettes from Sorghum panicle and pearl millets using a 20% starch binder	55.52	0	41.94	0	0.15	-	-	-	-	-	-	[71]
Briquettes from empty fruit bunch (EFB) fiber with corn starch binder	59.10	3.99	0.59	36.26	0.07	-	-	-	-	19.31	-	[61]

A high HHV typically correlates with a high content of carbon and hydrogen. A high carbon fraction also correlates with a high fixed carbon content, which enhances radiation heat transfer in the furnace, but also requires increased residence time to achieve complete combustion [68]. According to the data presented in Table 2, *BCP (9/1)* has the highest fixed carbon content, resulting in the highest HHV. Furthermore, the amount of air required for stoichiometric combustion of the nanocomposite fuels is also between 7.98 and 7.01 kg/kg of fuel, which is higher than the amount of air needed for wood fuel combustion (6 kg/kg fuel) [69].

Morphology

The morphology of the nanocomposite briquettes and starting materials is shown in Fig. 2. The micrographs showed that when the concentration of CNC in the biochar matrix increased, there was an evident increase in the recognized CNC domains. Furthermore, the surface of the biochar (Fig. 2(F)) is porous, which can contribute to the briquette's burning efficiency by providing additional routes for airflow, allowing more oxygen to circulate inside the briquette during combustion [55]. However, the pores were reduced/blocked with the addition of more binder, as expected, reducing the surface area and total pore volume of the nanocomposites [72].

Calorimetry

The calorific values of the nanocomposite fuel and starting materials are shown in Table 4. All of the nanocomposites have calorific values ranging from 23 to 27 MJ/kg, except BCP (5/5), which has a calorific value of 16 MJ/kg. The Tanzanian MEDC 12 (1323) DTZS standard requires carbonized fuels to have a minimum calorific value of 18 MJ/kg, hence BCP (5/5) would fail this test [45]. However, the European EN 1860-2:2005, the Ugandan US 765: 2007, and Kenyan DKS 2912: 2020 standards for charcoal and carbonized briquettes do not specify a minimum calorific value for the briquettes [44, 50, 57]. The calorific value of the briquettes in this study is also higher than those of previously developed biomass briquettes that utilized organic binders [18]. Notably, the calorific value of the nanocomposites decreased as the amount of binder increased, in line with the observation of Lubwama and others (2022) [7]. Based on the results of the t-test conducted with a significance level of $p=0.05$, a significant difference was observed between the higher heating values (HHV) obtained from the bomb calorimeter and those obtained from the ultimate analyzer for all the samples.

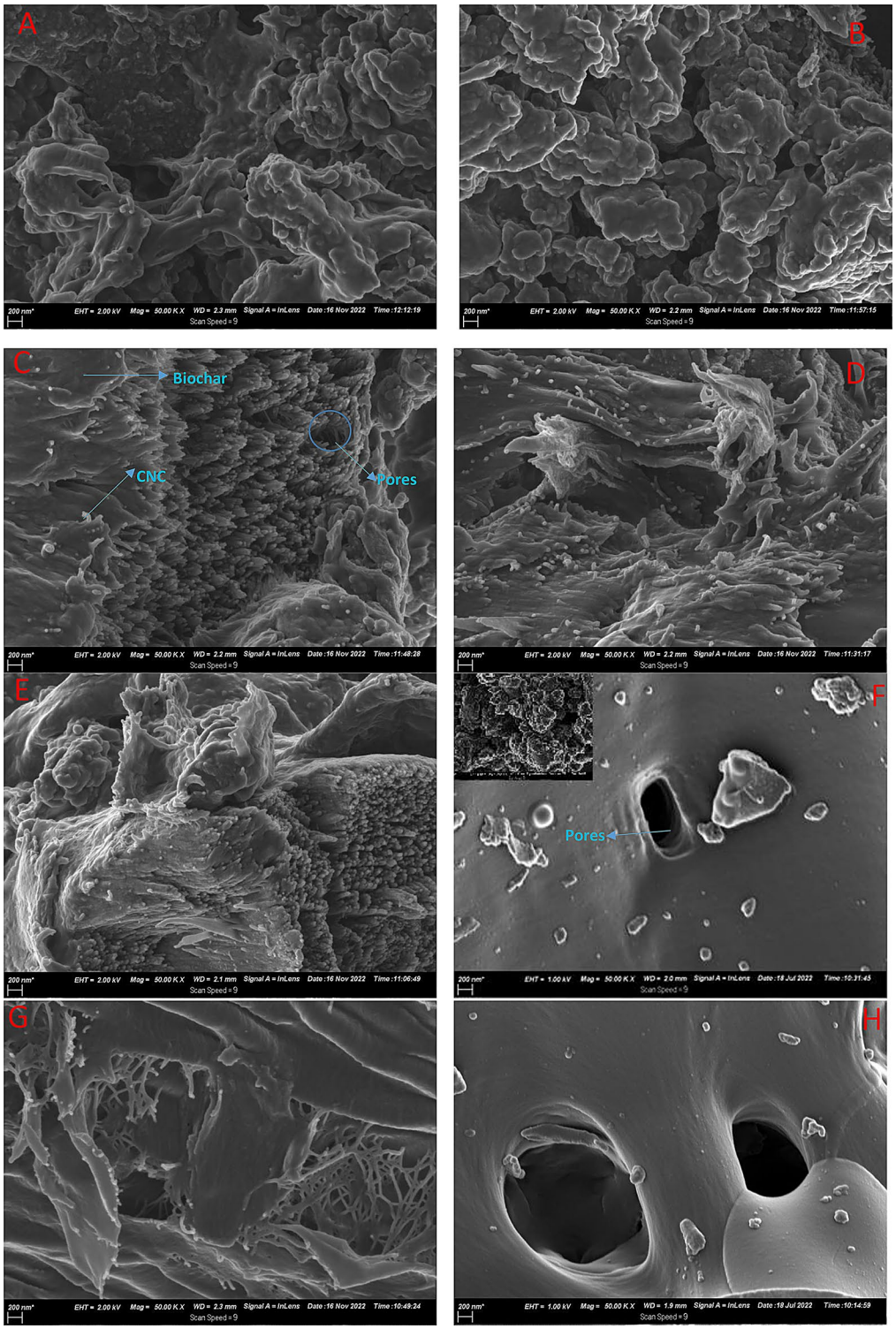

Fig. 2 SEM images of (**A**) BCP (9/1); (**B**) BCP (8/2); (**C**) BCP (7/3); (**D**) BCP (6/4); (**E**) BCP (5/5); (**F**) De-mineralized Biochar; (**G**) CNC; and (**H**) Biochar samples, respectively

Table 4 Heating value of selected samples

Sample	Higher heating value (MJ/kg)	Reference
BCP (9/1)	27.15±0.03	This study
BCP (8/2)	26.15±0.04	
BCP (7/3)	26.40±0.21	
BCP (6/4)	23.18±0.07	
BCP (5/5)	16.36±0.02	
De-mineralized Biochar	22.85±0.05	
CNC	14.43±0.16	
Carbonized Corn straw briquette with 40 wt % modified starch binder (Starch and NaOH)	25.23	[12]
Carbonized briquettes from groundnut shells and 30 g of cassava starch binder	23.90	[7]
Oil palm trunk bark uncarbonized briquettes with 10 wt % wastepaper pulp as a binder	16.71	[14]
Uncarbonized corn cob briquettes with 10 wt % wastepaper pulp as a binder	16.13	[14]
Sugarcane bagasse carbonized at 300 °C	33.45	[73]
Palm kernel shells carbonized at 400 °C	21.38	[73]
Carbonized empty fruit bunch briquette with Tapioca starch/water solution as a binder	23.62	[61]
Carbonized durian peel briquettes with tapioca glue as a binder	25.56	[18]

Elemental Composition

The elemental composition of the nanocomposites and starting materials is shown in Table 5. Carbon and Oxygen are the dominant elements in the nanocomposite fuel, in line with the observation of Adeleke et al.(2021) [74]. As the amount of binder increases, the carbon content of the nanocomposites decreases, in line with the observation of Oliveira et al.(2017) [75]. A high carbon content tends to form a high-grade biomass fuel suitable for combustion [76]. However, as the quantity of binder increases, the oxygen content increases. An increase in the oxygen content causes a decrease in the calorific value, collaborating with the results in Tables 3 and 4 [76]. Moreover, silicon plays a significant role along with oxygen bridges in improving the strength of the briquettes [59].

The combustion process is affected by inorganic elements, due to deposit formation, fly ash emissions, and their influence on the ash melting behavior [77, 78]. Furthermore, K, Na, Si, and Al lower the melting point of the ash, causing inorganic vapors to condense on the heat exchanger tube surface, generating fouling problems [78]. Additionally, Ca and Mg raise the ash melting point, which is beneficial for combustion [78]. The elemental composition of the nanocomposite briquettes is comparable to previously published data as shown in Table 5. The low fractions of inorganic elements in the nanocomposite fuels confirm their low ash content reported in Table 2 [36]. However, to evaluate the amount of inorganic elements in the nanocomposites to the existing ISO 17225-7 standard for non-woody briquettes and the ISO 17225-3 standard for wood briquettes, an ICP-OES experiment, is required [77].Unfortunately, this experiment could not be conducted at the time of this study.

Surface Chemistry

The FTIR spectra of the nanocomposite and starting materials are shown in Fig. 3. The nanocomposites' spectra shows the emergence of new peaks attributed to the CNC/PVA binder on the de-mineralized biochar. The broad band at 3331 cm^{-1} for the CNC, corresponds to the exposed

Table 5 Elemental composition of samples

Sample	Elements, Wt %										Reference
	C	O	Si	Ca	Cl	N	Al	Mg	K	Fe	
BCP (9/1)	74.08±1.81	25.43±1.86	0.24±0.34	0.03±0.02	0.27±0.09	-	-	-	-	--	This study
BCP (8/2)	72.82±1.20	26.57±1.35	0.07±0.05	0.09±0.05	0.46±0.13	-	-	-	-	-	
BCP (7/3)	71.47±1.55	28.05±1.55	-	0.05±0.05	*0.44*±0.06	-	-	-	-	-	
BCP (6/4)	70.87±13.41	28.52±13.26	0.09±0.05	0.13±0.07	0.39±0.19	-	-	-	-	-	
BCP (5/5)	63.45±3.27	36.06±3.47	0.08±0.05	0.16±0.11	0.27±0.14	-	-	-	-	-	
De-mineralized Biochar	70.20±13.03	13.68±8.78	-	-	0.18±0.09	15.95±6.77	-	-	-	-	
CNC	76.22±2.38	23.78±2.38	-	-	-	-	-	-	-	-	
Hybrid briquette from torrefied wood and coal fines with pitch as a binder	74.3	20.2	1.09	*0.92*	-	-	0.97	0.93	0.85	0.72	[74]
Briquette from sub-bituminous coal and torrefied biomass with 2% bentonite as a binder	~53	~11	~< 5	~< 5	~< 5	-	< 5	< 5	< 5	< 5	[59]

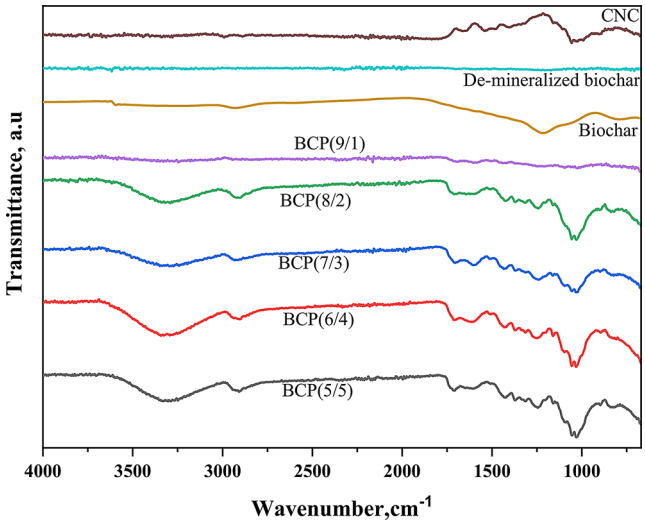

Fig. 3 FTIR spectra of the samples

hydroxyl groups of cellulose, which are bound by intermolecular hydrogen bonding [79]. The band at 1026 cm^{-1}, is associated with–C-O stretching of cellulose in the CNC. The presence of these functional groups promotes hydrogen bonding, which ensures interaction between the CNC and PVA for good adhesion and dispersion. The conversion of cellulose I to cellulose II, a more stable form of cellulose, is also linked to the band at 895 cm^{-1} for the CNC, which has an impact on the mechanical strength of the CNCs [79].

The broad band between 3000 cm^{-1} and 3600 cm^{-1} for the de-mineralized biochar is attributed to OH functional groups (alcoholic and phenolic). The band from 2700 cm^{-1} to 3000 cm^{-1} (peak center at 2929 cm^{-1} for the biochar sample) is attributed to alkyl C-H stretching. The peaks observed between 1760 cm^{-1} and 1650 cm^{-1} (peak center at 1699 cm^{-1}) are attributed to the acid axial deformation C=O, primarily aldehydes and ketones formed by dissociation of cellulose and hemicellulose. The peak at 1580 cm^{-1} is linked to aromatic C=C vibrations and C=O stretching. The band centered at 1222 cm^{-1} indicates the presence of C-O-C groups and aryl ethers, as well as aliphatic C-O stretching. The intense peak at 1207 cm^{-1} for the biochar sample is associated with the C-O-C stretching of ester groups in cellulose and hemicellulose. Additionally, the peak at 789 cm^{-1} is attributed to pyridine ring vibration and C-H deformation in the biochar [80–88]. The peak at 873 cm^{-1} is associated with the out-of-plane deformation produced by the aromatic C-H atom. The presence of these functional groups enhances the compatibility of the de-mineralized biochar with a matrix polymer [89].

The intensity of the FTIR peaks of the nanocomposite fuel varies with the PVA/CNC binder concentration. As the PVA/CNC binder content increases, the peak intensity increases too. The peaks between 2980 cm^{-1} -760 cm^{-1} are associated with =C-H, -OH-, C-N, -C=C-, N-H, C-O, C=O, and N-O bonds that indicate the presence of aromatic, aliphatic, saturated ethers, amines, nitro, tertiary and secondary hydroxyl groups [36, 55]. The presence of aliphatic and aromatic hydrocarbons in all the nanocomposites means that they contain fats and oils that are related to butane or isobutene, making it easier for the nanocomposites to burn or heat up. The peak at 3316 cm^{-1} is associated with the presence of hydroxyl groups that contribute to the flammability of the nanocomposites [55].

Thermal Stability

The thermogravimetric analysis (TGA) curves and the derivative thermogravimetric analysis (DTG) curves for all the samples are depicted in Fig. 4 (A &B) while a summary

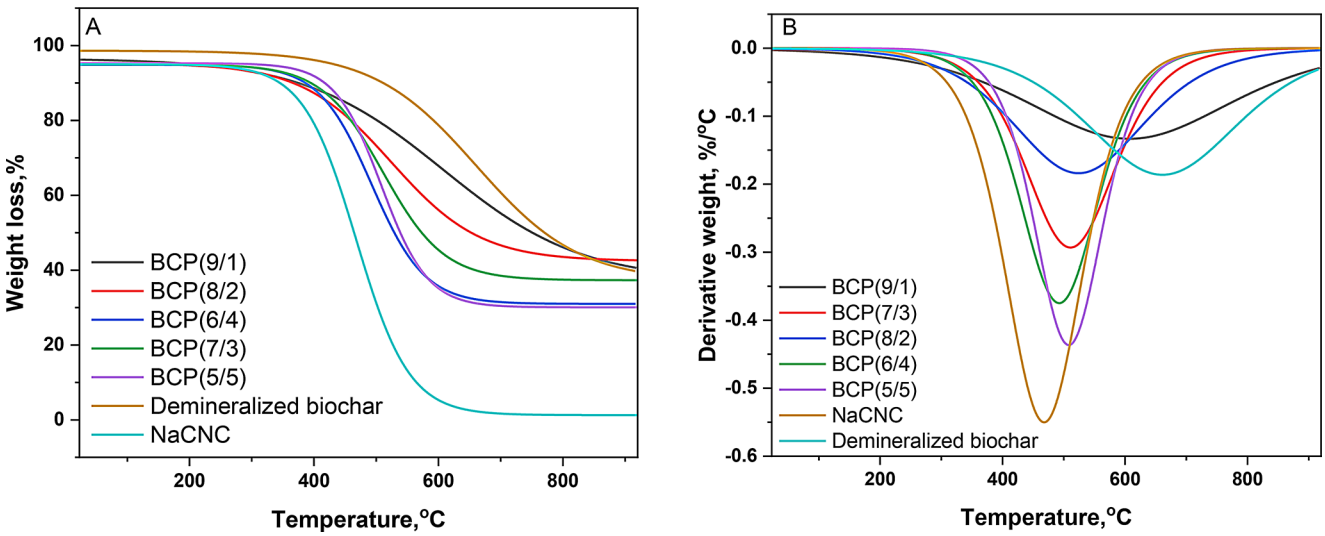

Fig. 4 (**A**) TGA and (**B**) DTG curves of selected samples

Table 6 Summary of TGA and DTG data

Samples	Moisture loss			Thermal decomposition				Residual char, %
	Δm, %	T_i, °C	T_f, °C	Δ m, %	T_i, °C	T_f, °C	T_p, °C	
BCP (9/1)	8.06	23.30	105.00	55.60	247.10	880.87	599.66	17.67
BCP (8/2)	5.60	25.40	104.15	44.71	379.53	656.91	507.19	17.70
BCP (7/3)	7.89	23.51	104.42	61.73	220.17	880.00	514.37	10.25
BCP (6/4)	8.21	23.30	105.13	68.34	370.99	912.97	491.02	19.02
BCP (5/5)	8.07	25.40	108.41	60.80	407.11	618.54	505.39	33.53
De-mineralized Biochar	6.88	25.54	105.30	55.72	270.41	908.71	612.56	19.15
CNC	4.65	37.99	101.82	85.47	304.02	404.16	350.64	-

Table 7 Combustion indices of nanocomposite fuel

Sample	FR	CI, MJ/kg	VI, MJ/kg	I_I	Reference
BCP (9/1)	0.59	53.43	24.39	58.20	This
BCP (8/2)	0.57	53.64	23.06	54.99	study
BCP (7/3)	0.41	75.90	24.19	57.73	
BCP (6/4)	0.28	97.50	20.94	49.98	
BCP (5/5)	0.21	91.32	13.30	31.74	
De-mineralized biochar	1.32	19.82	10.20	24.12	
CNC	0.03	580.37	14.20	33.92	
Terminalia	0.22	100.93	15.5		[93]
Torrefied wheat straw at 270 °C	0.57	34.58	18.68		
Corn husk and sawdust (9:1 blend ratio) briquettes using cassava starch as a binder	0.85	23	30.99		[91]
Peanut shells pyrolyzed at 400 °C	0.60	39.42	17.60		[36]
Sugarcane bagasse pyrolysed at 400 °C	0.55	39.99	18.05		[36]

of the weight loss (**Δ** m), onset temperature (T_i), final temperature (T_f) and peak temperature (T_p) of the two stages of thermal decomposition is presented in Table 6. The first stage of thermal decomposition occurs between 23 °C and 108 °C attributed to the dehydration process [36]. The second stage of thermal decomposition which occurs between 220 °C and 912 °C is attributed to coal combustion and devolatilization of lignin [36]. With the addition of the PVA/CNC nanocomposite binder, the peak temperature of the demineralized biochar also decreased.

The *BCP (7/3)* nanocomposite sample was the most thermally stable nanocomposite because it had the lowest onset degradation temperature (220 °C) and the highest peak temperature (514 °C). Due to its low concentration of inorganic chemicals (as shown in Table 5), which are often flame retardants, the sample also had the least amount of char residue [90].

Combustion Characteristics of Nanocomposite Briquettes

The fuel ratio (FR), combustibility index (CI), and volatile flammability (VI) of the nanocomposite fuels and starting materials are shown in Table 7. The fuel ratio of the nanocomposite fuels ranges between 0.59 − 0.21. A low FR suggests that the solid fuel easily ignites because of its high volatile matter content [91]. However, the combustion of biomass with high volatile matter content is rapid and difficult to control, resulting in the incomplete combustion of the fuel and the emission of smoke [91]. In coal-fired power plants, coals with FR in the range 0.5 to 3.0 are usually used; however, an FR greater than 2.0 causes ignition problems and flame instability [36, 91, 92]. Based on this index, only *BCP (9/1)*, and *BCP (8/2)* would qualify to be used as industrial fuels.

Additionally, the combustibility index (CI) is important for evaluating the suitability of specific biochar for blending with coal. The CI in the range from 12 MJ/kg − 23 MJ/kg is suitable, therefore all nanocomposite fuels would meet this criteria [91]. The volatile ignitability (VI) is a measure of available energy provided by the total volatiles (Volatile matter and moisture), assuming that the fixed carbon constituting the fuel sample is solely made up of pure carbon [91]. A VI value of at least 14 MJ/kg is desirable, hence all nanocomposite fuels would meet this criteria, except *BCP (5/5)* [92]. Moreover, the ignitability index of the nanocomposite fuels is also between 58 − 32. The ignitability index of most of the nanocomposite fuels is also better than that of biochar and the CNC. The recommended ignitability index of fuel applicable in thermal plants for power generation is 35, therefore only *BCP (5/5)* would not meet this criteria [38].

The TGA-DTG combustion profiles for the nanocomposite fuels in an oxygen environment are shown in Fig. 5 and a summary of the data is shown in Tables 8 and 9. The TGA graph describes three main stages of combustion. The first stage from 50 to 200 °C corresponds to the dehydration phase. The second phase from 200 to 400 °C is the

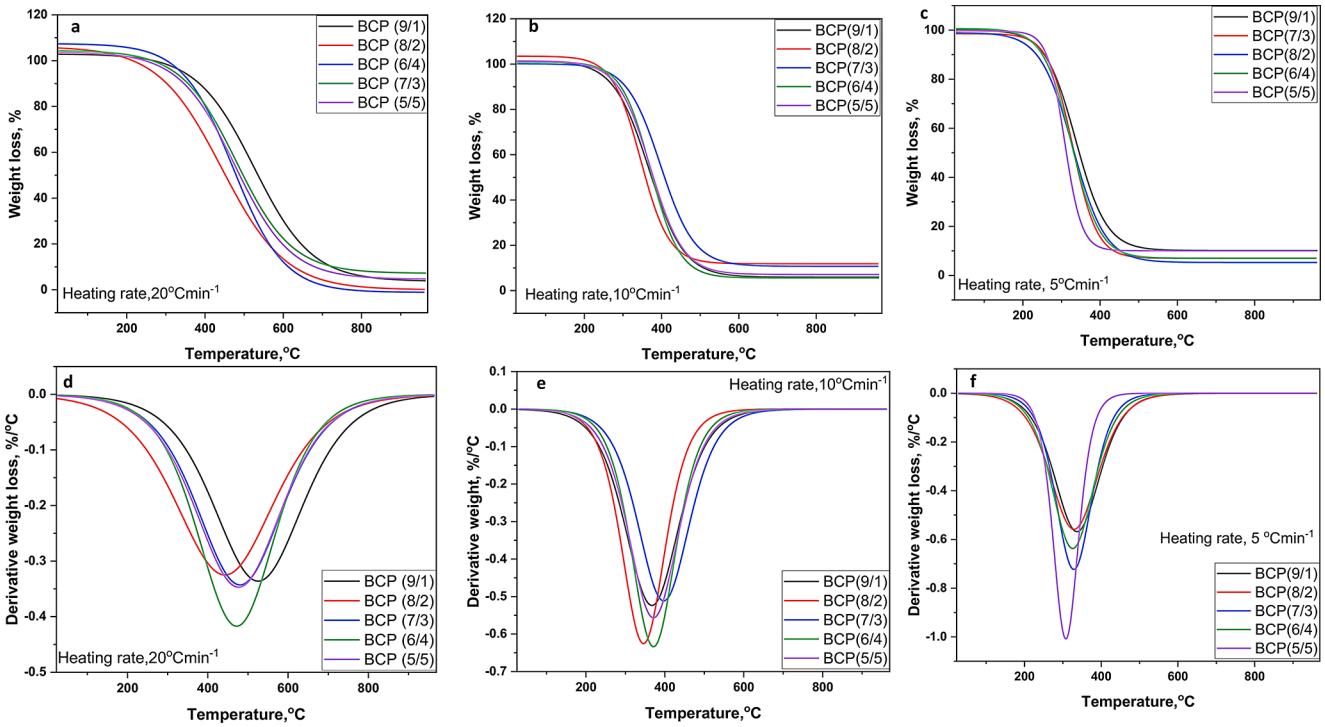

Fig. 5 (**a**), (**b**), (**c**) TGA, and (**d**), (**e**), (**f**) DTG combustion profiles for nanocomposite fuels at different heating rates</fig>

devolatilization phase, which occurs due to the degradation, release, and combustion of high volatile matter present in the nanocomposite fuels. The last stage between 500 and 960 °C is known as the char combustion phase, which occurs due to the combustion of fixed carbon retained in the nanocomposite fuel after venting all the volatile matter. After the completion of all stages, when there is no evident weight loss, the combustion reaches the burn-out phase [63, 94, 95].

According to the data presented in Table 8, an increase in heating rate from 5 °C/min to 20 °C/min leads to an increase in *Ti*, *Tp*, *Tf*, and the combustion rate. This suggests that there is an augmented transfer of heat from the surrounding environment to the interior of the sample per unit time. The intensified heat transfer significantly enhances the combustion rate of the fuel; however, it also results in shorter burnout time (*tf*), peak time (*tp*), and ignition time (*ti*) for the samples in line with observations of other authors [96]. The increase in heating rate also results in a decrease in the maximum weight loss of the nanocomposite fuels in line with previous observations [40]. The ignition temperature of all the briquettes at 5 °C/min is also lower than the ignition temperature of briquettes formed from PVA and coal fines reported by Botha and others, indicating enhanced ignitability [30].

A high value of ignition index (*Di*) is indicative of better ignition performance and lower ignition temperature [39, 97, 98]. According to the data in Table 9, *BCP (8/2)* exhibits the highest *Di* value at a heating rate of 20 °C/min and 10 °C/min, suggesting superior ignition performance compared to the other five nanocomposite briquettes. This sample also has the lowest ignition temperature at all heating rates, in line with previous observations [39, 98].

The burnout index D_f is used to describe the burnout characteristics of the nanocomposite fuel. Sample *BCP (6/4)* had the highest D_f at 20 °C/min, hence requiring the least time and temperature to complete burnout at the same heating rate among the nanocomposite fuels. The presence of minerals in fuels has been noted to enhance burnout performance by acting as oxygen carriers that promote oxygen transfer to the inside of the fuel [39]. Based on the data in Table 5, it is evident that *BCP (6/4)* exhibits the highest mineral content, closely followed by *BCP (8/2)*, which aligns with the observed elevated D_f values within the samples.

The index of comprehensive combustion characteristic, *S*, reflects the ignition, combustion, and burnout properties of the sample [99]. A value greater than 2×10^{-7} $min^{-2} \cdot K^{-3}$ indicates good general burning performance of the fuel [100]. The *S* values range between 1.43 and 2.99×10^{-7} $min^{-2} \cdot K^{-3}$ for the nanocomposite fuels, with *BCP (6/4)* having the highest value followed by *BCP (8/2)*. The indices at heating rates of 10 °C/min and 5 °C/min, are both below 2×10^{-7} $min^{-2} \cdot K^{-3}$, indicating inadequate combustion performance for the nanocomposite fuels under these specific heating conditions.

Table 8 Summary of TGA and DTG data for combustion profiles of nanocomposite fuel at different heating rates

Heating rate, °Cmin^{-1}	Ignition temperature, T_i, °C			Peak temperature, T_p, °C			Burnout temperature, T_f, °C			Maximum combustion rate, mgmin^{-1}			Ignition time, t, min			Peak time, t_p, min			Burn out time, t_f, min		
	20	10	5	20	10	5	20	10	5	20	10	5	20	10	5	20	10	5	20	10	5
BCP (9/1)	369.83	269.57	260.29	525.78	371.50	338.45	684.08	468.86	424.17	4.19	2.46	1.25	6.28	25.84	45.46	12.16	36.67	62.74	18.47	47.39	80.25
BCP (8/2)	276.86	262.23	243.67	440.59	345.39	329.13	611.61	429.79	415.10	4.74	2.62	1.46	4.59	24.59	43.71	9.89	34.92	59.31	16.08	45.11	75.31
BCP (7/3)	340.06	304.98	259.86	480.01	391.93	328.61	620.88	493.05	398.91	4.06	2.28	1.57	5.44	26.87	47.62	10.34	36.10	62.09	15.50	45.34	77.38
BCP (6/4)	328.84	286.42	251.01	472.06	371.46	325.78	609.67	455.91	398.04	5.57	2.89	1.49	6.57	26.13	44.43	11.14	34.42	60.45	15.50	42.32	77.06
BCP (5/5)	319.57	279.94	254.98	476.14	367.79	308.06	624.55	464.98	362.85	4.56	3.04	2.14	6.57	25.84	41.95	11.22	34.02	52.87	16.08	42.54	65.01

The index of intensity, H_f describes the rate and intensity of combustion [39]. A low H_f value reflects a good combustion performance. The H_f values for the nanocomposite fuels range from 1.37 to 1.79. *BCP (6/4)* has the lowest H_f value of 1.37 at 20 °C/min, showing that it has the highest intensity of combustion. On the other hand, *BCP (9/1)* had the highest H_f value of 1.79, signifying poor reactivity of the fuel but stable combustion [39, 98].

The flammability index C is used to evaluate the combustion stability of the nanocomposite fuel. The range of C indices of the nanocomposite fuels lies between 6.57 and 12.72×10^{-5}, with *BCP (8/2)* having the highest index, followed by *BCP (6/4)*. Hence *BCP (8/2)* has the highest combustion stability [39]. Based on the analysis of nanocomposite combustion in an oxygen environment, *BCP (6/4)* and *BCP (8/2)* exhibited superior combustion properties compared to other nanocomposite fuels. Nonetheless, the influence of the nanocomposite binder transcends mere additive effects, contributing to the intricate nature of the combustion dynamics within the nanocomposite fuel.

Combustion Kinetics of Nanocomposite Fuels

The kinetic parameters of the nanocomposite fuels are shown in Table 10 and the Arrhenius curves in Fig. 6. The correlation coefficients were in the range of 0.9950–0.9999. The correlation coefficients are higher than 0.92, hence high accuracy of results [41, 101]. The activation energies were calculated using the Coats–Redfern method. The activation energies were lowered as the heating rate was decreased from 20 to 5 °C/min. At 5 °C/min, *BCP (7/3)* had the least activation energy of 13.30 kJmol^{-1}, hence the least amount of energy required for the initiation reaction. Nevertheless, it is essential to ascertain the kinetic parameters at various heating rates below 8 °C/min. This is necessary to address the intricacies associated with the decomposition of lignocellulosic biomass, as the combustion process generates a substantial amount of heat that can lead to uncontrolled sample combustion at higher heating rates [102, 103].

The pre-exponential factor (A) describes the number of molecules with effective collision. A high pre-exponential factor indicates a rapid reaction rate at low activation energy, which is the trend observed for all the nanocomposite fuels [104, 105]. An increase in the pre-exponential factor quickens the reaction rate, so there is a compensation effect between the pre-exponential factor and activation energy [105]. The compensation effect has been theorized to be caused by several factors including non-uniformity of the surface and formation of unstable transitional products during combustion [105, 106].

Table 9 Combustion characteristic indexes of nanocomposite fuels at different heating rates

Heating rate, °Cmin^{-1}	DTG_{mean}, wt%/min			DTG_{max}, wt%/min			$\Delta T_{½}$, °C			$\Delta t_{½}$, min			$D_i \times 10^{-3}$, wt%/min^3			$D_f \times 10^{-3}$, wt%/min^{-4}			$S \times 10^{-7}$, wt %/min$^{2°}$C^3			H_f, °C			$C \times 10^{-5}$, wt %/min^1°C^2		
	20	10	5	20	10	5	20	10	5	20	10	5	20	10	5	20	10	5	20	10	5	20	10	5	20	10	5
BCP (9/1)	6.30	4.77	2.73	8.99	5.02	2.82	271.69	158.93	139.20	9.52	16.63	28.14	4.39	5.30	0.99	4.21	0.17	0.02	6.05	7.03	2.68	1.79	1.28	1.32	6.57	6.91	4.16
BCP (8/2)	6.29	5.49	2.74	9.75	5.99	2.78	292.20	128.88	148.50	8.80	15.80	25.91	7.16	6.98	1.07	6.97	0.24	0.02	13.08	11.27	3.09	1.50	1.06	1.31	12.72	8.71	4.68
BCP (7/3)	6.87	4.77	3.27	9.59	4.88	3.60	262.43	154.82	112.44	9.12	15.99	25.31	6.10	5.03	1.22	6.56	0.19	0.03	9.18	5.08	4.37	1.59	1.35	1.13	8.29	5.25	5.33
BCP (6/4)	7.57	5.69	3.16	12.66	6.08	3.17	229.93	133.09	129.38	7.50	13.29	25.97	5.70	6.76	1.18	9.77	0.31	0.03	14.54	9.24	3.99	1.37	1.15	1.21	11.71	7.41	5.03
BCP (5/5)	6.49	5.07	4.15	9.86	5.34	5.03	250.46	149.96	77.96	9.03	12.82	17.82	4.68	6.08	2.27	6.05	0.29	0.08	10.03	7.43	8.84	1.54	1.22	0.84	9.65	6.81	7.73

Mechanical Properties

The stress-strain curve for the nanocomposite samples and a summary of the mechanical tests are shown in Fig. 7; Table 11 respectively. The *BCP (7/3)* nanocomposite has the highest Young's modulus (105 MPa) and Ultimate tensile strength (11 MPa). The briquettes must have a minimum compressive strength of 2.56 MPa to avoid breakage during handling and storage, hence only *BCP (9/1)* would fall short of this requirement [109]. Moreover, the minimum compressive strength required for commercial charcoal briquettes is 0.375 MPa [110]. Therefore, *BCP (9/1)* can still be utilized for cooking applications that do not involve extensive handling, storage, or transportation. Furthermore, increasing the binder content is generally expected to enhance the compressive strength of briquettes [111]. However, previous studies have reported that binder concentrations exceeding 18% may negatively impact strength, though the underlying mechanisms for this trend remain unclear [112]. In this study, the compressive strength continued to improve with increasing binder content, reaching an optimal level at 30% nanocomposite binder within the char matrix.

According to the technical specifications of the European standard for solid biofuels in the form of briquettes, the briquettes must have a density value of at least 500 kgm^{-3} [75]. A high briquette density is advantageous for transportation as it enhances structural integrity, reducing the risk of fragmentation during handling and storage [75]. Except for *BCP (9/1)*, all briquettes would also satisfy this requirement. Furthermore, besides binder type and concentration, the other factors that affect mechanical properties of the briquettes are process variables like the die diameter, die temperature, pressure, and pre-heating of the biomass mix [17]. These variations introduce challenges in making direct comparisons between the mechanical properties of the nanocomposite briquettes and those reported in the literature.

Conclusion

A novel biochar briquette with a CNC/PVA nanocomposite binder, developed at varying biochar/binder ratios, is reported in this study. The moisture content, volatile matter content, and fixed carbon content of the briquettes increased as the amount of binder was increased, thereby agreeing with previous information obtained in literature on other briquettes. The elemental analysis also shows that the principal components of all the nanocomposite briquettes prepared and characterized in this study were carbon and oxygen. The *BCP (7/3)* nanocomposite briquette displayed the highest thermal stability, least char residue, and highest compressive strength of 11 MPa. All the nanocomposite

Table 10 Kinetic parameters for nanocomposite fuels at different heating rates

Heating rate		20°Cmin^{-1}			10°Cmin^{-1}			5°Cmin^{-1}			Reference
	Combustion stage	**E, kJmol^{-1}**	**A, min^{-1}**	**R^2**	**E, kJmol^{-1}**	**A, min^{-1}**	**R^2**	**E, kJmol^{-1}**	**A, min^{-1}**	**R^2**	This study
BCP (9/1)	Stage 1*	35.55	6.49×10^{-5}	1	14.82	4.28×10^{-4}	0.9699	13.77	3.75×10^{-4}	0.9690	
	Stage 2*	11.72	2.66×10^{-3}	1	9.44	4.49×10^{-3}	0.9566	44.90	1.01×10^{-5}	0.9654	
	Stage 3*	-	-	-	-	-	-	6.74	8.07×10^{-3}	0.9920	
BCP (8/2)	Stage 1	29.65	1.14×10^{-4}	1	17.09	3.47×10^{-4}	0.9618	15.24	1.75×10^{-4}	0.9645	
	Stage 2	9.18	4.37×10^{-3}	1	11.12	3.35×10^{-3}	1	53.09	1.56×10^{-6}	0.9569	
	Stage 3	-	-	-	-	-	-	6.64	7.48×10^{-3}	0.9963	
BCP (7/3)	Stage 1	22.38	2.13×10^{-4}	0.9723	16.55	3.60×10^{-4}	0.9722	13.30	4.10×10^{-4}	0.9673	
	Stage 2	8.92	4.71×10^{-3}	1	7.04	8.16×10^{-3}	0.9955	52.46	3.51×10^{-6}	0.9615	
	Stage 3	-	-	-	-	-	-	6.67	9.05×10^{-3}	0.9943	
BCP (6/4)	Stage 1	18.91	2.42×10^{-4}	0.9886	19.53	1.73×10^{-4}	0.9643	15.47	2.61×10^{-4}	0.9824	
	Stage 2	14.28	9.78×10^{-4}	0.9920	7.84	6.79×10^{-3}	0.9946	57.04	1.13×10^{-6}	0.9544	
	Stage 3	-	-	-	-	-	-	6.80	8.47×10^{-3}	0.9909	
BCP (5/5)	Stage 1	35.30	7.80×10^{-5}	0.9345	23.91	1.63×10^{-4}	0.9793	15.27	3.27×10^{-4}	0.9809	
	Stage 2	8.58	5.21×10^{-3}	1	8.15	6.64×10^{-3}	0.9860	64.95	1.96×10^{-7}	0.9801	
	Stage 3	-	-	-	-	-	-	6.79	7.58×10^{-3}	0.9899	
Raw Coal					91.39						[39]
Biochar blend (20% biochar and 80% coal)	Stage 1 Stage 2	25.34 29.68		0.9934 0.9947							[107]
Hydrochar from sewage sludge at 320 °C	Stage 1(150–260 °C) Stage 2 (300–550 °C)				28.98 32.60	14.50 22.70					[108]

*Approximate temperature ranges for different combustion stages: Stage 1 (290–550 °C), Stage 2 (550–750 °C), Stage 3 (750 °C -1240 °C[a])

[a] extrapolated beyond experimental range of 950 °C

briquettes met the required minimum compressive strength for commercial charcoal, hence they can be stored and transported without fragmentation. The maximum heating value was recorded for the *BCP (9/1)* nanocomposite briquette at 27 MJ/kg, while *BCP (8/2)* and *BCP (7/3)* were not dissimilar with 26 MJ/kg. Additionally, the three nanocomposites satisfied all the criteria for the combustion indices; *BCP (9/1)*, *BCP (8/2)*, and *BCP (7/3)*.

The nanocomposite briquettes developed in this study have a very low ash content in comparison to previously reported briquettes from agricultural residues that utilized organic or inorganic binders as seen in Table 2. Consequently, there is an opportunity to produce biomass fuels of high quality that utilize CNC/PVA nanocomposites as a binder for household and industrial applications. The majority of the briquettes satisfied the global and regional standards for carbonized briquette, especially *BCP (7/3)* which satisfied all these standards. However, scale-up studies of this process depend on an in-depth understanding of the influence of parameters such as pyrolysis temperature and time, compaction pressure, and extrusion method on the yield and quality of the produced briquette. These factors should be investigated for optimum conditions before scale-up studies are carried out. Since the commercial viability of this process and the product obtained thereof depends on the comprehensive economic assessment of the process and the product (i.e. CNC synthesis from biomass and the production of the biopolymer-based briquette), it is recommended that a comprehensive economic feasibility study be carried out.

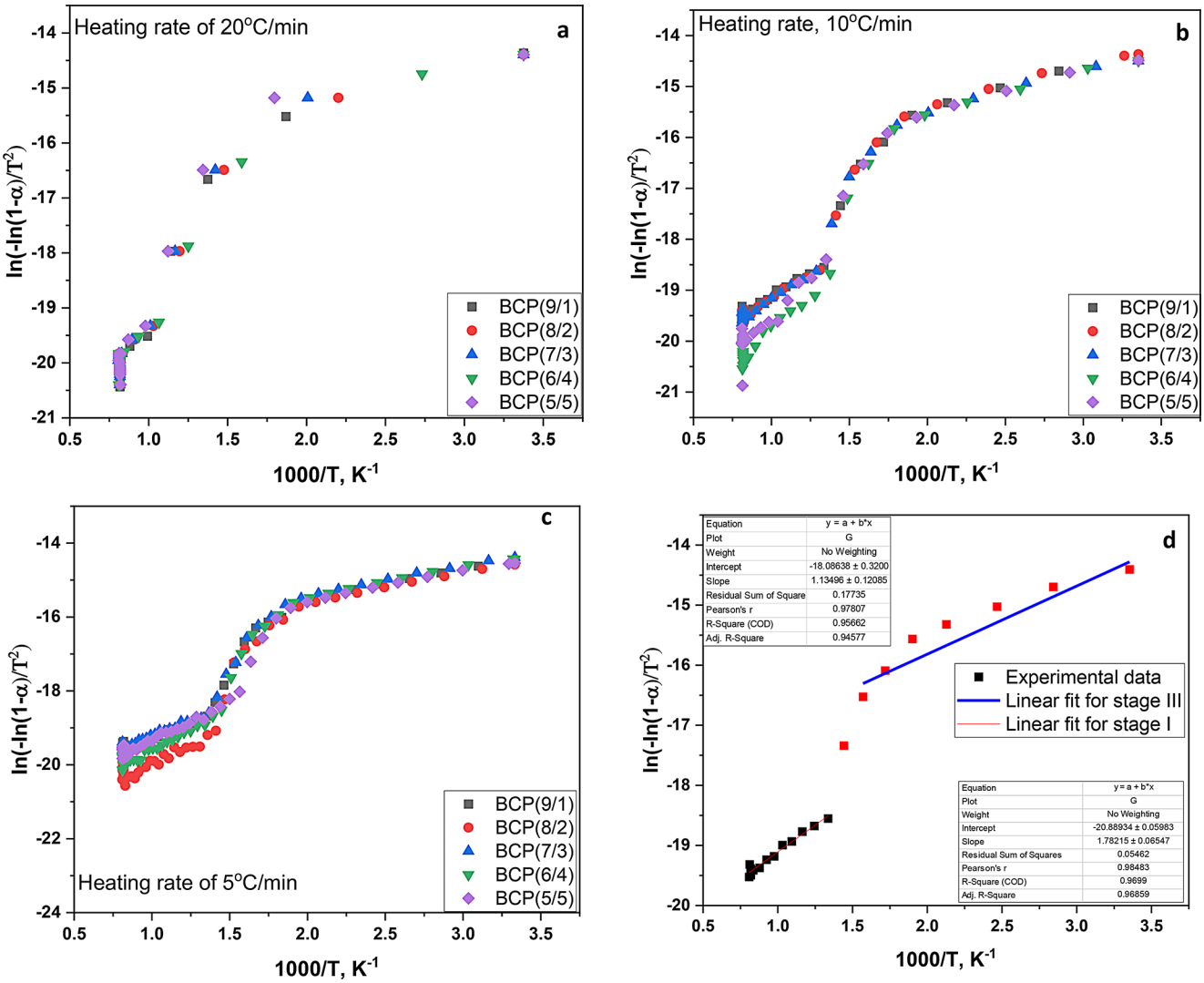

Fig. 6 Fitted lines for Arrhenius curves for nanocomposite fuels at different heating rates (**a**) 20 °Cmin-1(**b**)10°Cmin-1 (**c**)5°Cmin-1 (d)illustration of data fitting</fig>

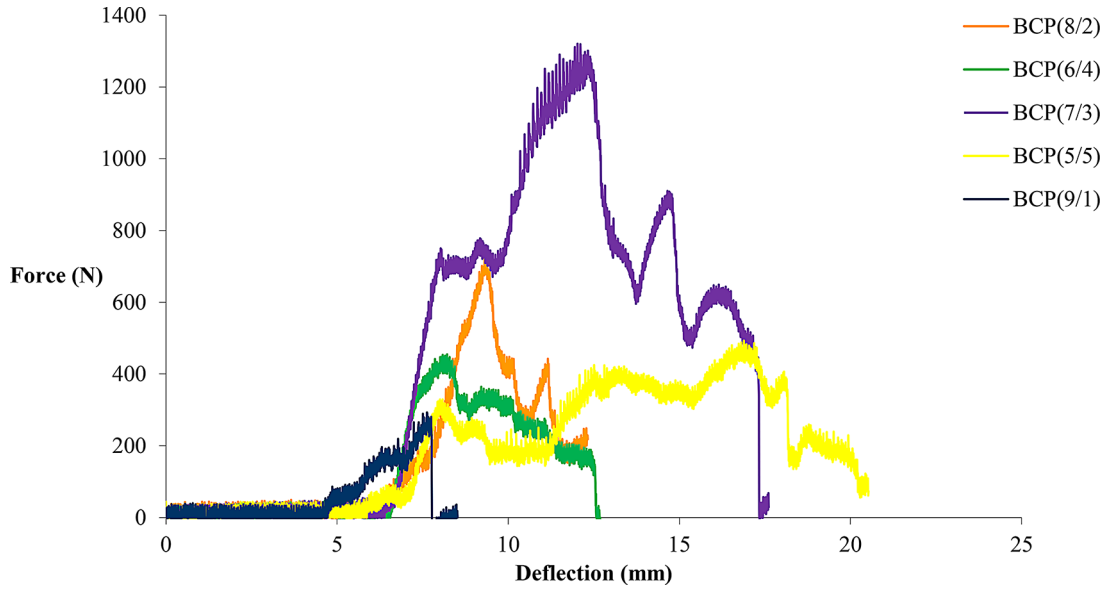

Fig. 7 Stress-strain curve for briquette samples

Table 11 Summary of mechanical test results

Sample	Young's modulus, MPa	Ultimate tensile strength, MPa	Density, kg/m^3	Reference
BCP (9/1)	2.30	2.14	413.91	This study
BCP (8/2)	40.87	5.798	844.20	
BCP (7/3)	104.54	10.59	747.46	
BCP (6/4)	89.78	3.43	627.37	
BCP (5/5)	74.94	5.19	720.84	
Charcoal briquettes from water hyacinth with molasses as a binder (70:30 ratio)	-	1.87	840	[55]
Briquettes from durian peels and coconut shells carbonized at 300 °C with starch as a binder	-	1.25×10^{-3}	850	[113]
Briquettes from charcoal fines and resin from Canarium Schweinfurthii as a binder	-	10.94	1036	[109]
Briquette produced from sewage sludge and charcoal fines (50:50 ratio) using glue flour as a binder	41.19	-	388	[75]

Author Contributions All authors contributed to the successful completion of this study. Ayaa Fildah, Kabir Oyedotun, Michael Lubwama, Samuel Ayodele Iwarere, Michael Olawale Daramola, and John Baptist Kirabira conceptualized the project and reviewed the first draft. Michael Olawale Daramola, Samuel Ayodele Iwarere and John Baptist Kirabira were responsible for supervision, funding acquisition and project administration.

Funding Open access funding provided by University of Pretoria. This work was supported by the African Center of Excellence in Materials, Product Development and Nanotechnology (MAPRONANO ACE) funded by the World Bank and Government of Uganda [Project Identification P151847, IDA Number 5797-UG]. Additionally, Ayaa Fildah acknowledges the support she received from The Prof. Daramola Development Fund which enabled her to complete her laboratory work at the University of Pretoria.

Data Availability The datasets are available upon reasonable request from the corresponding author.

Declarations

Conflict of Interest The authors declare no conflict of interest.

References

1. Stoner, O., et al.: Household cooking fuel estimates at global and country level for 1990 to 2030. Nat. Commun. **12**(1), 5793 (2021)
2. Puthumana, J.S., et al.: Risk factors for cooking-related burn injuries in children, WHO global burn registry. Bull. World Health Organ. **99**(6), 439 (2021)
3. Kumar, P., Igdalsky, L.: Sustained uptake of clean cooking practices in poor communities: Role of social networks. Energy Res. Social Sci. **48**, 189–193 (2019)

4. WHO. Household air pollution [cited 2023 15/02/2023] (2023). Available from: https://www.who.int/news-room/fact-sheets/detail/household-air-pollution-and-health
5. International Energy Agency (IEA), I.R.E.A.I., United Nations Statistics Division (UNSD), World Bank, and the World Health Organization (WHO): Tracking SDG7 Access to Clean Cooking (2022)
6. Bakehe, N.P., Hassan, R.: The effects of access to clean fuels and technologies for cooking on deforestation in developing countries. J. Knowl. Econ., 1–17 (2022)
7. Lubwama, M., Yiga, V.A., Lubwama, H.N.: Effects and interactions of the agricultural waste residues and binder type on physical properties and calorific values of carbonized briquettes. Biomass Convers. Biorefinery. **12**(11), 4979–4999 (2022)
8. Dinesha, P., Kumar, S., Rosen, M.A.J.E.T.: Biomass briquettes as an alternative fuel: A comprehensive review. Review **7**(5), 1801011 (2019)
9. Zhang, G., Sun, Y., Xu, Y.: Review of briquette binders and briquetting mechanism. Renew. Sustain. Energy Rev. **82**, 477–487 (2018)
10. Husain, Z., Zainac, Z., Abdullah, Z.: Briquetting of palm fibre and shell from the processing of palm nuts to palm oil. Biomass Bioenerg. **22**(6), 505–509 (2002)
11. Amaya, A., et al.: Activated carbon briquettes from biomass materials. Bioresour. Technol. **98**(8), 1635–1641 (2007)
12. Guo, Z., et al.: Characteristics of biomass charcoal briquettes and pollutant emission reduction for sulfur and nitrogen during combustion. Fuel. **272**, 117632 (2020)
13. Kumar, J.A., et al.: Comparative analysis of briquettes obtained from biomass and charcoal. Materials Today Proc. **45**, 857–861 (2021)
14. Kpalo, S.Y., et al.: Production and characterization of hybrid briquettes from corncobs and oil palm trunk bark under a low pressure densification technique. Sustainability. **12**(6), 2468 (2020)
15. Ferronato, N., et al.: Are waste-based briquettes alternative fuels in developing countries? A critical review. Energy. Sustain. Dev. **68**, 220–241 (2022)
16. Nandiyanto, A.B.D., Azizah, N.N., Girsang, G.C.S.: Optimal design and Techno-economic analysis for corncob particles briquettes: A literature review of the utilization of agricultural waste and analysis calculation. Appl. Sci. Eng. Progress. **15**(3), 5508–5508 (2022)
17. Kpalo, S.Y., et al.: A review of technical and economic aspects of biomass briquetting. Sustainability. **12**(11), 4609 (2020)
18. Sanchez, P.D.C., Aspe, M.M.T., Sindol, K.N.: An overview on the production of Bio-briquettes from agricultural wastes: Methods, processes, and quality. J. Agricultural Food Eng. **1**, 2716–6236 (2022)
19. Espinoza-Tellez, T., et al.: Agricultural, forestry, textile and food waste used in the manufacture of biomass briquettes: A review. Scientia Agropecuaria. **11**(3), 427–437 (2020)
20. Waheed, M., Akogun, O., Enweremadu, C.: An overview of torrefied bioresource briquettes: quality-influencing parameters, enhancement through torrefaction and applications. Bioresources Bioprocess. **9**(1), 1–18 (2022)
21. Kalema, J., et al.: Undocumented invasive exotic Woody plants of Mabira central forest reserve, Uganda. Afr. J. Ecol. **60**(4), 1110–1119 (2022)
22. Ayaa, F., et al.: Potential of invasive shrubs for energy applications in Uganda. Energy Ecol. Environ. **7**(6), 563–576 (2022)
23. Ndwandwa, N., et al.: Extraction and characterization of cellulose nanofibers from yellow thatching grass (Hyparrhenia filipendula) straws via acid hydrolysis. Waste Biomass Valoriz. **14**(8), 2599–2608 (2023)
24. Obi, O.F., Pecenka, R., Clifford, M.J.: A review of biomass briquette binders and quality parameters. Energies. **15**(7), 2426 (2022)
25. Shu, M.Y., Yin, H.Y., Liu, G.H.: Experimental researches on composite bentonite-based briquette binder. Adv. Mater. Res. **496**, 276–280 (2012)
26. Benk, A., Delibaş, A., Çoban, A.: Economical biobinders and their blends suitable for the production of coal briquettes, heat insulating materials and other industrial applications. Int. J. Coal Preparation Utilization. **42**(11), 3484–3501 (2022)
27. Patra, S.K., et al.: Synthesis of bio-polymer based composite binder for utilization of industrial coke dust waste. Fuel. **311**, 122502 (2022)
28. Henning, C., et al.: Testing of Briquettes made From Witbank Coal Fines with Polyvinyl Alcohol as Binder (2018)
29. Rajput, S., Thorat, B.: Recovered Polyvinyl alcohol as an alternative binder for the production of metallurgical quality coke breeze briquettes. Int. J. Coal Preparation Utilization. **42**(3), 475–485 (2022)
30. Botha, D., et al.: Evaluation of polymer binders in briquetting of coal fines for combustion applications. J. South Afr. Inst. Min. Metall. **121**(3), 113–118 (2021)
31. Liu, S., et al.: High strength clean briquettes production from long-flame coal fines by using Polyvinyl alcohol and coal slime as binders. Asia-Pacific J. Chem. Eng. **15**(2), e2414 (2020)
32. Guo, Z., et al.: Optimization of composite binder for lignite powder briquetting. Int. J. Coal Preparation Utilization. **42**(10), 2990–3003 (2022)
33. Wang, Q., et al.: Fabrication of densified rice husk by sequential hot-compressed water treatment, blending with Poly (vinyl alcohol), and hot pressing. ACS Omega. **7**(31), 27638–27648 (2022)
34. Ji, H., et al.: Strategy towards one-step Preparation of carboxylic cellulose nanocrystals and nanofibrils with high yield, carboxylation and highly stable dispersibility using innocuous citric acid. Green Chem. **21**(8), 1956–1964 (2019)
35. Liu, W., et al.: Highly efficient and sustainable Preparation of carboxylic and thermostable cellulose nanocrystals via FeCl3-catalyzed innocuous citric acid hydrolysis. ACS Sustain. Chem. Eng. **8**(44), 16691–16700 (2020)
36. Hadey, C., et al.: Preparation and characterization of biochars obtained from biomasses for combustible briquette applications. Sci. World J. **2022** (2022)
37. Conag, A.T., et al.: Energy densification of sugarcane Bagasse through torrefaction under minimized oxidative atmosphere. **5**(6), 5411–5419 (2017)
38. Adeleke, A., et al.: The ignitability, fuel ratio and Ash fusion temperatures of torrefied Woody biomass. Heliyon. **6**(3), e03582 (2020)
39. Tang, L., et al.: Thermogravimetric analysis of the combustion characteristics and combustion kinetics of coals subjected to different chemical demineralization processes. ACS Omega. **7**(16), 13998–14008 (2022)
40. Garcia, E., Ejim, I.F., Liu, H.: Thermogravimetric analysis of co-combustion of a bituminous coal and coffee industry by-products. Thermochim. Acta. **715**, 179296 (2022)
41. Jia, G.: Combustion characteristics and kinetic analysis of biomass pellet fuel using thermogravimetric analysis. Processes. **9**(5), 868 (2021)
42. Cao, W., Li, J., Lue, L.: Study on the ignition behavior and kinetics of combustion of biomass. Energy Procedia. **142**, 136–141 (2017)
43. Onchieku, J.M., Chikamai, B.N., Rao, M.: Optimum parameters for the formulation of charcoal briquettes using Bagasse and clay as binder. Eur. J. Sustainable Dev. **1**(3), 477–477 (2012)

44. KEBS: Solid Biofuel —Sustainable Charcoal and Carbonized Briquettes for Household and Commercial use — Specification. Kenya Bureau of Standards (2020)
45. TBS: Solid biofuel — Sustainable Charcoal and Carbonized Briquettes for Household and Commercial use — Specification. Tanzania Bureau of Standards (2022)
46. Petrović, S., Glavonjić, G.: Standards and certificates for charcoal and charcoal briquettes in the function of harmonization of their quality and market development. In: Proceedings of the Development Trends in Economic Management in Wood Processing and Furniture Manufacturing, Kozina, Slovenia, p. 9 (2011)
47. Inegbedion, F., Ikpoza, E.: Estimation of the moisture content, volatile matter, ash content, fixed carbon and calorific values of rice husk briquettes. In: Proceedings of the International Conference on Industrial Engineering and Operations Management Nsukka, Nigeria (2022)
48. Afsal, A., et al.: Experimental investigations on combustion characteristics of fuel briquettes made from vegetable market waste and saw dust. Mater. Today: Proc. **33**, 3826–3831 (2020)
49. Akowuah, J.O., Kemausuor, F., Mitchual, S.J.: Physico-chemical characteristics and market potential of sawdust charcoal briquette. Int. J. Energy Environ. Eng. **3**, 1–6 (2012)
50. UNBS: Wood Charcoal and Charcoal Briquettes for Household use — Specification. Uganda National Bureau of Standards (2007)
51. Veeresh, S.J., Narayana, J.: Assessment of agro-industrial wastes proximate, ultimate, SEM and FTIR analysis for feasibility of solid bio-fuel production. Univ. J. Env. Res. Technol. **2**(6) (2012)
52. Kebede, T., Berhe, D.T., Zergaw, Y.: Combustion characteristics of briquette fuel produced from biomass residues and binding materials. J. Energy. **2022**(1), 4222205 (2022)
53. Alzahrani, A., Hassan, M.A., Alsubaie, S.: Evaluating the properties that affect the quality of the charcoal product, determining the limits of toxic emissions during combustion, and studying their impact on human health. Environ. Geochem. Health. **46**(8), 295 (2024)
54. Miao, M., et al.: Effects of volatile matter and oxygen concentration on combustion characteristics of coal in an oxygen-enriched fluidized bed. Energy. **220**, 119778 (2021)
55. Carnaje, N.P., et al.: Development and characterisation of charcoal briquettes from water hyacinth (Eichhornia crassipes)-molasses blend. PloS One. **13**(11), e0207135 (2018)
56. Ige, A.R., et al.: The effect of binder ratio on the physical and combustion characteristics of carbonized rice stalk briquettes. Int. J. Adv. Acad. Res. (Sciences Technol. Engineering), **6**(10) (2020)
57. AENOR: Appliances, solid fuels and firelighters for barbecuing-Part 2: Barbeque charcoal and barbeque charcoal briquettes. Requirements and test methods (2003)
58. Bagabo, P., Scufield, T.: Uganda's Oil Refinery: Gauging the Government's Stake. Natural Resource Governance Institute (2024)
59. Adeleke, A., et al.: Briquetting of subbituminous coal and torrefied biomass using bentonite as inorganic binder. Sci. Rep. **12**(1), 8716 (2022)
60. Mengesha, A., et al.: Characterization and production of briquettes fuel from brewery wastewater sludge and sawdust. Waste Dispos. Sustainable Energy. **4**(3), 243–256 (2022)
61. Nazari, M., Idroas, M., Ayuni, F.: Carbonization effect on EFB briquettes prepared with different type of binders. In: IOP Conference Series: Earth and Environmental Science. IOP Publishing (2020)
62. Ab Jalil, N.A., et al.: Physical and chemical characteristics of Agricultural-Plastic wastes for feasibility of solid fuel briquette production. Sustainability. **14**(23), 15751 (2022)
63. Aliyu, M., Iwabuchi, K., Itoh, T.: Improvement of the fuel properties of dairy manure by increasing the biomass-to-water ratio in hydrothermal carbonization. Plos One. **17**(7), e0269935 (2022)
64. Shen, Y., et al.: Hydrothermal carbonization of medical wastes and lignocellulosic biomass for solid fuel production from lab-scale to pilot-scale. Energy. **118**, 312–323 (2017)
65. Tomen, W.T., et al.: Physical and combustion properties investigation of hybrid briquettes from tropical sawdust: Case study of Iroko (Milicia excelsa) and Padouk (Pterocarpus soyauxii). Energy Rep. **9**, 3177–3191 (2023)
66. Tiyawongsakul, T.: Non-reacting Flow Characteristics and Emissions Reduction on Blends of Coal and Dairy Biomass in 30 kW_ (t) Low NO_ (x) Down-Fired Furnace (2014)
67. Yang, S., et al.: Comprehensive Estimation of combustion behavior and thermochemical structure evolution of four typical industrial polymeric wastes. Energies. **15**(7), 2487 (2022)
68. Mendoza Martinez, C.L., Sermyagina, E., Vakkilainen, E.: Hydrothermal carbonization of chemical and biological pulp mill sludges. Energies. **14**(18), 5693 (2021)
69. Nega, T., et al.: Biomass energy conversion in a gasifier for Injera baking Mitad application. Heliyon. **8**(12), e12128 (2022)
70. Dragusanu, V., Lunguleasa, A., Spirchez, C.: Evaluation of the physical, mechanical, and calorific properties of briquettes with or without a Hollow made of wheat (Triticum aestivum L.) straw waste. Appl. Sci. **12**(23), 11936 (2022)
71. Velusamy, S., et al.: Comparative analysis of agro waste material solid biomass briquette for environmental sustainability. Adv. Mater. Sci. Eng. **2022** (2022)
72. Leng, L., et al.: An overview on engineering the surface area and porosity of Biochar. Sci. Total Environ. **763**, 144204 (2021)
73. Nunes, L.J., et al.: Evaluation of the potential of agricultural waste recovery: Energy densification as a factor for residual biomass logistics optimization. Appl. Sci. **11**(1), 20 (2020)
74. Adeleke, A., et al.: Physical and mechanical characteristics of composite briquette from coal and pretreated wood fines. Int. J. Coal Sci. AndTechnology. **8**, 1088–1098 (2021)
75. de Oliveira, R.S., et al.: Briquettes production for use as power source for combustion using charcoal thin waste and sanitary sewage sludge. Environ. Sci. Pollut. Res. **24**(11), 10778–10785 (2017)
76. Kimutai, S.K., Kimutai, I.K.: Investigation of physical and combustion properties of briquettes from cashew nut shell and cassava binder. Int. J. Educ. Res. **7**(11), 15–26 (2019)
77. Senila, L., et al.: Characterization of biobriquettes produced from vineyard wastes as a solid biofuel resource. Agriculture. **12**(3), 341 (2022)
78. Moreno, A.I., Font, R., Conesa, J.A.: Physical and chemical evaluation of furniture waste briquettes. Waste Manage. **49**, 245–252 (2016)
79. Pavalaydon, K., Ramasawmy, H., Surroop, D.: Comparative Evaluation of Cellulose Nanocrystals from Bagasse and Coir agro-wastes for Reinforcing PVA-based Composites, pp. 1–22. Environment, Development and Sustainability (2022)
80. Askeland, M., Clarke, B., Paz-Ferreiro, J.: Comparative characterization of biochars produced at three selected pyrolysis temperatures from common Woody and herbaceous waste streams. PeerJ. **7**, e6784 (2019)
81. Azzaz, A.A., et al.: Olive mill by-Products thermochemical conversion via hydrothermal carbonization and slow pyrolysis: Detailed comparison between the generated hydrochars and biochars characteristics. Processes. **10**(2), 231 (2022)
82. Zhao, S.-X., Ta, N., Wang, X.-D.: Effect of temperature on the structural and physicochemical properties of Biochar with Apple tree branches as feedstock material. Energies. **10**(9), 1293 (2017)

83. Tomczyk, A., Sokołowska, Z., Boguta, P.: Biochar physicochemical properties: Pyrolysis temperature and feedstock kind effects. Reviews Environ. Sci. Bio/Technology. **19**(1), 191–215 (2020)
84. Li, X., et al.: Characterization of biochars from Woody agricultural wastes and sorption behavior comparison of cadmium and atrazine. Biochar. **4**(1), 1–12 (2022)
85. Liu, Y., He, Z., Uchimiya, M.: Comparison of Biochar formation from various agricultural by-products using FTIR spectroscopy. Mod. Appl. Sci. **9**(4), 246 (2015)
86. Armynah, B., et al.: *Potentials of biochars derived from bamboo leaf biomass as energy sources: effect of temperature and time of heating.* Int. J. Biomater. **2019** (2019)
87. Janu, R., et al.: Biochar surface functional groups as affected by biomass feedstock, Biochar composition and pyrolysis temperature. Carbon Resour. Convers. **4**, 36–46 (2021)
88. Alfattani, R., et al.: Bio-char characterization produced from walnut shell biomass through slow pyrolysis: Sustainable for soil amendment and an alternate bio-fuel. Energies. **15**(1), 1 (2021)
89. Behazin, E., et al.: Mechanical, chemical, and physical properties of wood and perennial grass biochars for possible composite application. BioResources. **11**(1), 1334–1348 (2016)
90. Fu, S., Song, P., Liu, X.: Thermal and flame retardancy properties of thermoplastics/natural fiber biocomposites. In: Advanced High Strength Natural Fibre Composites in Construction, pp. 479–508. Elsevier (2017)
91. Akogun, O.A., et al.: Physical and combustion indices of thermally treated cornhusk and sawdust briquettes for heating applications in Nigeria. J. Nat. Fibers. **19**(4), 1201–1216 (2022)
92. Conag, A.T., et al.: Energy densification of sugarcane Bagasse through torrefaction under minimized oxidative atmosphere. J. Environ. Chem. Eng. **5**(6), 5411–5419 (2017)
93. Akogun, O., Waheed, M.: Property upgrades of some raw nigerian biomass through torrefaction pre-treatment-a review. J. Phys. Conf. Ser. (2019)
94. Venna, S., et al.: Landfill leachate as an alternative moisture source for hydrothermal carbonization of municipal solid wastes to solid biofuels. Bioresour. Technol. **320**, 124410 (2021)
95. Kijo-Kleczkowska, A., et al.: Comparative thermal analysis of coal fuels, biomass, fly Ash and polyamide. Energy. **258**, 124840 (2022)
96. Liu, J., et al.: Combustion kinetics characteristics of solid fuel in the sintering process. Processes. **8**(4), 475 (2020)
97. Sahu, S.G., et al.: Thermogravimetric assessment of combustion characteristics of blends of a coal with different biomass Chars. Fuel Process. Technol. **91**(3), 369–378 (2010)
98. Mureddu, M., et al.: Air-and oxygen-blown characterization of coal and biomass by thermogravimetric analysis. Fuel. **212**, 626–637 (2018)
99. Yuanyuan, Z., et al.: Investigation of combustion characteristics and kinetics of coal gangue with different feedstock properties by thermogravimetric analysis. Thermochim. Acta. **614**, 137–148 (2015)
100. Wang, C., et al.: Thermogravimetric studies of the behavior of wheat straw with added coal during combustion. Biomass Bioenerg. **33**(1), 50–56 (2009)
101. Buratti, C., et al.: Thermogravimetric analysis of the behavior of sub-bituminous coal and cellulosic ethanol residue during co-combustion. Bioresour. Technol. **186**, 154–162 (2015)
102. Wnorowska, J., Ciukaj, S., Kalisz, S.: Thermogravimetric analysis of solid biofuels with additive under air atmosphere. Energies. **14**(8), 2257 (2021)
103. Osman, A.I., et al.: Physicochemical characterization and kinetic modeling concerning combustion of waste berry pomace. ACS Sustain. Chem. Eng. **8**(47), 17573–17586 (2020)
104. Plis, A., Lasek, J., Skawińska, A.: Kinetic analysis of the combustion process of Nannochloropsis Gaditana microalgae based on thermogravimetric studies. J. Anal. Appl. Pyrol. **127**, 109–119 (2017)
105. Yang, G., et al.: Combustion characteristics and kinetics study of pulverized coal and semi-coke. High Temp. Mater. Processes (London). **38**(2019), 783–791 (2019)
106. Li, Q.-W., et al.: Thermokinetic characteristics of coal spontaneous combustion based on thermogravimetric analysis. Fuel. **250**, 235–244 (2019)
107. Yousaf, B., et al.: Systematic investigation on combustion characteristics and emission-reduction mechanism of potentially toxic elements in biomass-and biochar-coal co-combustion systems. Appl. Energy. **208**, 142–157 (2017)
108. He, C., et al.: Utilization of sewage-sludge-derived hydrochars toward efficient cocombustion with different-rank coals: Effects of subcritical water conversion and blending scenarios. Energy Fuels. **28**(9), 6140–6150 (2014)
109. Kivumbi, B., et al.: Production of carbonized briquettes from charcoal fines using African elemi (Canarium schweinfurthii) resin as an organic binder. In: Energy Sources, Part A: Recovery, Utilization, and Environmental Effects, pp. 1–17 (2021)
110. Ward, B.J., Yacob, T.W., Montoya, L.D.: Evaluation of solid fuel Char briquettes from human waste. Environ. Sci. Technol. **48**(16), 9852–9858 (2014)
111. Aransiola, E., et al.: Effect of binder type, binder concentration and compacting pressure on some physical properties of carbonized corncob briquette. Energy Rep. **5**, 909–918 (2019)
112. Rubio, B., Izquierdo, M., Segura, E.: Effect of binder addition on the mechanical and physicochemical properties of low rank coal Char briquettes. Carbon. **37**(11), 1833–1841 (1999)
113. Sari, E., et al.: Studies of carbonization process on the production of durian peel biobriquettes with mixed biomass coconut and palm shells. In: IOP Conference Series: Materials Science and Engineering. IOP Publishing (2018)